

# Solar InfraRed COronal Magnetograph

(SIRCOM)



Proposal for a space based coronagraph for vector  
magnetic field measurements

# Solar InfraRed COronal Magnetograph (SIRCOM)

A joint proposal by PRL & ISAC for a solar vector  
coronal magnetograph submitted for

ESA COSMIC VISION

Prepared by Shibu K. Mathew

15 June 2007

Team members

PRL

Shibu K. Mathew  
Nandita Srivastava  
Sanjay Gosain  
Brajesh Kumar  
A. Raja Bayanna  
P. Venkatakrisnan

ISAC

K. Sankarasubramanian

## **Abstract**

We propose a space based solar coronagraph for the vector magnetic field measurements. A space based coronagraph is highly desirable in order to avoid the earth's atmospheric scattered light related problems in coronal magnetic field measurements. There are several interesting problems which could be addressed by knowing the vector magnetic field in the corona. Some of the most interesting problems are, the magnetic field configuration for the origin of coronal mass ejections, role of magnetic field in the coronal heating, and solar g-mode detection. There are a handful of lines in the infrared wavelength which could be used for the coronal magnetic measurements, among those Fe XIII line is the most suitable line for this purpose. For the magnetic field measurements using this line, we describe the expected polarization signal level and the measurement technique employed to retrieve the polarization signals. Towards the end, we discuss the optical layout of a space based coronagraph and the magnetograph.

## Table of contents

|  |           |
|--|-----------|
| <b>1. Introduction</b>   | <b>2</b>  |
| <b>2. Justification for space based measurements</b>   | <b>4</b>  |
| <b>3. Science goals and observational requirements</b>   | <b>6</b>  |
| 3.1. Coronal Mass Ejections (CMEs).....  | 6         |
| 3.2. Coronal heating.....  | 6         |
| 3.3. Solar g-mode detection.....   | 7         |
| <b>4. Suitability of Fe XIII (1.0746<math>\mu</math>m) line for coronal magnetic field measurement</b> | <b>8</b>  |
| <b>5. Expected polarization signals from Fe XIII coronal line</b>                                      | <b>9</b>  |
| <b>6. Polarization measurement technique</b>   | <b>10</b> |
| <b>7. Wavelength selection: Narrow band tunable birefringent filter</b>                                | <b>13</b> |
| <b>8. Photon budget and exposure time estimation</b>   | <b>14</b> |
| <b>9. Preliminary optical design of the coronagraph</b>  | <b>15</b> |
| 9.1. Telescope (Coronagraph).....  | 15        |
| 9.2. Back end instrument (Coronal magnetograph).....   | 16        |
| 9.2.1. Calibration optics.....   | 16        |
| 9.2.2. Polarimeter.....  | 17        |
| 9.2.3. Narrow band filter.....   | 17        |
| 9.2.4. IR detector.....  | 18        |
| 9.2.5. Instrument control and data acquisition system.....   | 18        |
| <b>10. Satellite requirement</b>   | <b>18</b> |
| <b>11. Time schedule</b>   | <b>19</b> |
| <b>References</b>  | <b>19</b> |

## 1. Introduction

The magnetic pressure exceeds the thermal pressure in the solar corona ( $\beta = P_{th}/P_m \ll 1$ ), and thus all plasma flows are governed by the magnetic field. This results in an extremely inhomogeneous corona which is filled with thin magnetic flux tubes of different densities and temperature. Figure 1 show images of the corona taken in soft X-ray and EUV wavelengths. The images display structured and complex loops which presumably follow the magnetic field lines.

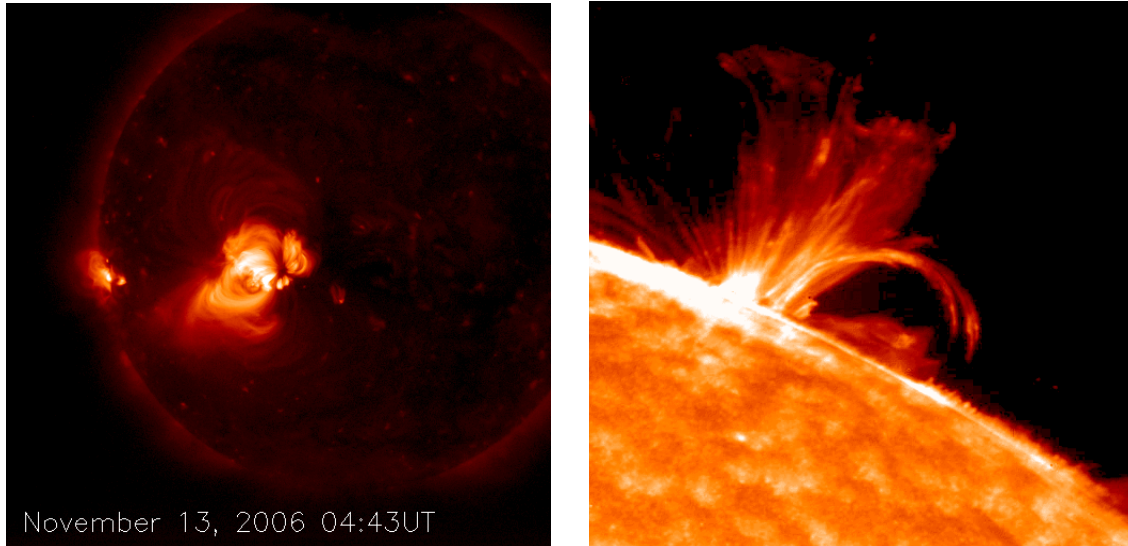


**Fig. 1.** Coronal structures seen in X-ray and EUV images. These images are taken by *Hinode XRT telescope* and *TRACE EUV imager*.

It is believed that most of the dynamical processes occurring in the solar corona are directly related to the magnetic field. The examples of such dynamic processes are coronal heating, CMEs and solar flares. Understanding the origin of these phenomena require consistent, long duration magnetic field measurements at the sites of those events. Measurement of coronal magnetic field is one of the challenging problems in solar physics. The problem basically arises due to the very small field strengths (only of the order of few Gauss) at the coronal heights.

There exist several methods which could be used for measuring the coronal magnetic field, a list of which can be found in Judge et al.<sup>[1]</sup> The two most promising techniques which could be used for the measurement are based on Hanle effect and the Zeeman effect. Hanle effect is a quantum interference effect occurring when the splitting between the atomic levels caused by the magnetic field is of the same order as the natural damping width of the spectral line. This effect is manifested as rotation and depolarization of linearly polarized light which is originally generated by the resonant scattering in the spectral lines. The Lyman  $\alpha$  (1215Å) line is considered as a suitable candidate for the Hanle measurements<sup>[2]</sup>. But, the quantum theory to understand the problem of frequency-

dependent resonant scattering has not been fully developed for this line, which makes the interpretation of the measurements, difficult.

Longitudinal Zeeman effect in the coronal emission lines (CEL) have been used in the past for coronal magnetic field measurements<sup>[3,4]</sup>. Due to the requirement of highly sensitive polarimetry, low-scatter instrument and low sky background most of the past measurements are inconclusive. Recently Lin et al.<sup>[5,6]</sup> reported coronal magnetic field observations using a 0.46m off-axis reflecting coronagraph in conjunction with optical fiber-bundle imaging spectro-polarimeter and obtained a field strength of around 4G in an active region about 100arc-sec above the solar limb. Figure 2 shows the line-of-sight magnetic field contour overlotted on the EIT Fe XV image and few Stokes V profiles for the same region from the above observations.

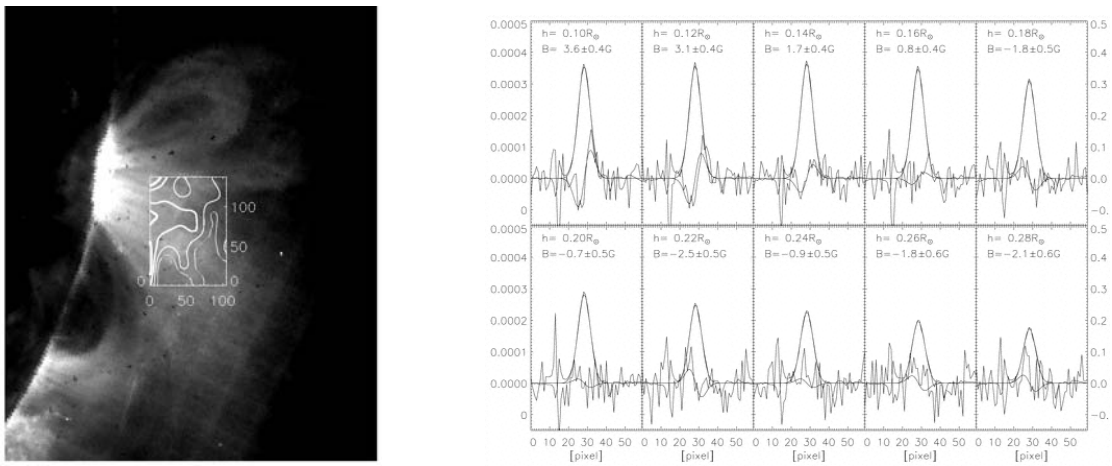


**Fig 2.** Coronal magnetic field measurement from Lin et al.<sup>[6]</sup> **Left:** The magnetic field contours over-plotted on EIT Fe XV image. The thick contour is for 4G and the additional contours are for 2,0, and -2G. **Right:** Few of the fitted Stokes V and I profiles with the measurements from the same region.

The measurement shown above is carried out in the infrared coronal emission line of Fe XIII at 1075nm, for 70 minutes of integration with a 20 arc-sec pixel resolution. This successful observation shows the usefulness of Zeeman effect for the coronal magnetic field measurement. But, looking at the feeble and noisy Stokes V profiles, it also reminds us of the difficulty in obtaining these measurements.

Infrared emission lines are potential candidates for coronal vector magnetic field measurements through Zeeman effect and its direction projected onto plane of the sky through the resonance polarization. The wavelength dependence of Zeeman splitting i.e.  $\Delta\lambda \propto \lambda^2 B$ , makes the infrared lines more sensitive to magnetic field than the visible lines. A list of useful coronal emission lines and their theoretical diagnostic properties are described in a series of papers by Judge and co-authors.<sup>[7,8,9,10]</sup> In conclusion, full Stokes polarimetry (Stokes I, Q, U, V measurements) in an appropriate coronal emission line can provide crucial information on the magnetic field strength and direction, which is

indispensable to understand the various dynamic processes taking place in the solar corona.

In this report, we propose a space-based coronagraph for magnetic field measurements which can be a part of European Space Agency's (ESA) 'Cosmic Vision' theme. The polarization properties of Fe XIII coronal infrared emission line at 1075nm through Stokes polarimetry will be used for the measurements. In the following sections, we give justification for space based measurements, list the science goals, describe the technique and present the preliminary layout of the instrument.

**Summary:** *Measurement of coronal magnetic field is crucial to understand the dynamic processes happening in the solar corona. Stokes polarimetry using Fe XIII infrared line at 1075nm can provide this vital information.*

## 2. Justification for space based measurements

Coronal brightness is much lower than that of the solar disk. The continuum corona is almost a million times fainter than the solar disk intensity, in the isolated coronal emission lines the average intensity can be one order better. Ground based coronal intensity measurements face a major problem from the earth's atmosphere. The Earth's atmosphere scatters the disk light into the coronal intensity which makes it difficult to observe the corona. Figure 3 shows the scattered light intensity levels for various sky conditions compared with the coronal intensities. E-corona represents integrated emission from coronal lines. The individual, isolated coronal emission lines are one to two orders brighter, and even then it could only be observed in exceptional sky and seeing conditions.

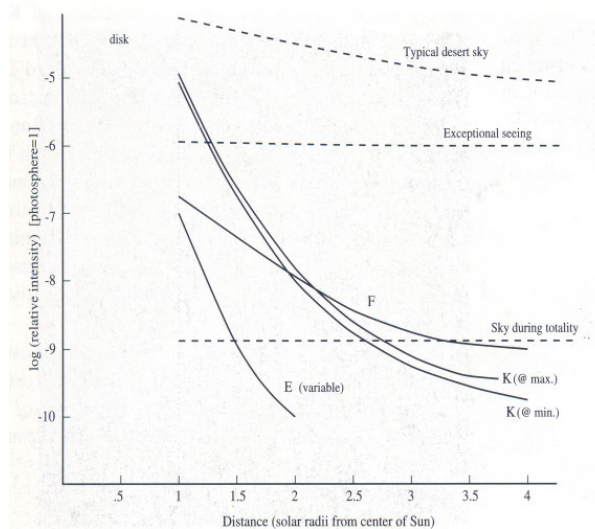


**Fig. 3.** *Brightness variation of the main components of the solar corona as a function of radial distance. Adapted from L. Golub and J. M. Pasachoff (Book: The Solar Corona)*

The dominant sources of stray light produced in the atmosphere are the Rayleigh scattering from the molecules and scattering from aerosols. The scattered light is linearly polarized and can introduce problems in the measurement of  $Q$  and  $U$  and, through cross-talk in  $V$  Stokes profiles of the emission lines.

Since the coronal magnetic field measurements involve very accurate Stokes polarimetry, long integration time is required to build-up the signal. A stable and exceptionally good sky condition is essential for ground based observatory to pursue these measurements. Also, the linear polarization introduced by the scattering make the analysis of the Stokes profiles complicated. For understanding the dynamical behavior of the corona, evolution of magnetic field in the corona must be studied, which requires continuous and long duration observations. Few ground based observatories (NSO, SacPeak, HAO, Hawaii) make routine intensity observations in white light or in coronal emission lines. Only recently, reliable magnetic field measurements are reported by Lin et al.<sup>[6]</sup> using a dedicated telescope (SOLARC) and infra-red spectro-polarimeter. CoMP<sup>[21]</sup> is another filter based instrument which demonstrated the coronal magnetic field measurements. The scarcity of the above kind of observations reminds us of the difficulty in making these measurements. The 4m ATST (NSO) telescope and COSMO (HAO) are planned ground based observatories, which will be carrying out the coronal magnetic field measurements in future, but with restricted polarimetric accuracies due to atmosphere.

The problem of scattered light introduced by the Earth's atmosphere can be completely eliminated in a space based instrument. In particular, measuring coronal magnetic field from space has the following advantages ;

- No scattered light produced by the atmosphere,
- No variable atmospheric air mass,
- No variable seeing conditions,
- No linear polarization introduced by atmospheric scattering,
- No dust related telescope scattering,
- Continuous visibility of the Sun (in appropriately chosen orbit)

It is therefore quite evident that, in order to understand the dynamic processes happening in the solar corona, a space based coronagraph capable of magnetic field measurement is fully justified. As far as we know, there is only one proposed space mission KuaFu, which 'might' carry an instrument capable of coronal magnetic field measurements using Hanle effect<sup>[2]</sup>.

**Summary:** *Ground based coronal magnetic field observations suffer from atmospheric scattered light, variable seeing conditions and mixing up of linear polarization produced by atmospheric scattered light. All the above can be completely avoided in a space based coronagraph.*

### 3. Science goals and observational requirements

#### 3.1. Coronal Mass Ejections (CMEs)

Coronal mass ejections (CMEs) are sporadic eruptions of large plasma structures into the interplanetary space, which carry mass in the range of  $10^{14}$  -  $10^{16}$  g. CMEs can severely disrupt the Earth's environment. These intense radiations and particles from the Sun can alter the Earth's outer atmosphere, can seriously affect satellite orbits, and disrupt long distance radio communications and navigation systems. Understanding the origin and propagation of CMEs is one of the important factors involved in the "space weather" prediction.

Theory and observations clearly indicate that the magnetic field provides the energy that drives CMEs<sup>[11,12,13,14]</sup>. But the exact knowledge of the field structure and the mechanism for eruption remain controversial. Most of the theoretical models deal with the magnetic system generated by the dynamo in the solar interior, which then emerges through the photosphere to the corona, and carries significant magnetic helicity (twists and linkage of magnetic field lines). The helicity gets accumulated due to the twists produced by the photospheric evolution or due to the new flux emergence. The field structure in the corona evolves to a state when the self confinement of the closed structure fails and a CME like explosion occurs.

Due to the unavailability of direct coronal magnetic field measurements, observational studies mostly concentrate on the changes in the photospheric magnetic field which is believed to be related to the initiation and eruption of the CMEs. Majority of these studies are inconclusive. Another method used is the extrapolation of the photospheric magnetic field to the coronal heights. This technique is also subjected to several problems. For example, except in the case of potential field configuration, the mathematical problem associated with the extrapolation is an ill-posed boundary value problem in which small errors in the photospheric magnetic measurements grow exponentially. This stresses the need for the direct coronal (vector) magnetic field measurements to understand the conditions that leads to energy build-up and eruption in CMEs. The measurement will also validate different CME models and will allow to directly compare the photospheric magnetic field extrapolations.

**Observational requirement:** *High temporal and spatial resolution measurements of magnetic field strength and direction (vector field) in the solar corona/coronal loops. This could be achieved by high sensitivity Stokes polarimetry in a chosen coronal emission line.*

#### 3.2. Coronal heating

Heating of solar corona remains one of the major puzzles in solar physics. Observing the coronal emission lines originating from highly ionized atoms, a temperature of  $\approx 1$  MK was inferred in the corona. Comparing this coronal temperature with photospheric

temperature of 6000K, corona is almost 200 times hotter. If thermal conduction is the only cause for coronal heating, the temperature in the corona should drop down from the chromospheric value with increasing distance, which is not the case. Therefore, unfolding the mystery of coronal heating mechanism is one of the important tasks in coronal physics.

Several theoretical models exist which deal with the coronal heating. In most of the models, coronal heating is treated as a multi-stage process<sup>[15]</sup>, which consist of a mechanical driver providing the initial energy, an electro-magnetic coupling of the energy to the locations of magnetic energy storage followed by magnetic instability and loss of equilibrium. The last stage is the energy release and transport which heats-up the plasma. Photospheric granular and super granular flows are considered to be providing the initial energy. In ‘DC’ heating models, these flows twist the magnetic field lines which wrap around each other and energy is dissipated between the twisted field lines<sup>[16]</sup>. In ‘AC’ heating models, the heating process basically occurs as a result of propagating Alfvén waves. Whenever the time scale of the wave excitation is shorter than the Alfvén travel time (which depends on the magnetic field strength in the coronal structure) back and forth in the coronal structure the wave propagates. The energy flux carried by the Alfvén waves is sufficient to heat the coronal holes, quiet Sun regions and coronal loops (in this case it is a slightly different mechanism – resonant absorption). Accurate measurement of coronal magnetic field (both magnitude and direction) is important test any of the above models. Until now, observational studies were mainly focused on the evolution of photospheric magnetic field its correlation with the active region coronal heating<sup>[17,18]</sup>, but this is only a part of the story.

**Observational requirement: High temporal and spatial resolution measurements of magnetic field strength and direction (vector field) in the solar corona/coronal loops along with full line profiles for temperature diagnostics. Again, this could be achieved by high sensitivity Stokes spectro-polarimetry in a chosen coronal emission line.**

### 3.3. Solar g-mode detection

*g-modes* are low frequency internal gravity oscillations, with periods of  $\approx 30$  minutes and longer. These oscillations are primarily confined to Sun’s radiative interior, and the observation of these oscillations could provide a lot of information about the core which is otherwise very little probed by the *p-modes* (acoustic waves).

Conventional way of detecting solar *g-modes* relies on the “tunneling” of the *g-modes* through the evanescent portion in the convection zone. This results in extremely low amplitudes of the *g-modes* on the solar surface. Recent upper limits have been put as 10mm/s in velocity, and below 0.5 parts per million in intensity<sup>[19]</sup>. However, Thomson et al<sup>[20]</sup> detected *g-mode* signatures in interplanetary magnetic field fluctuations, which has not received widespread acceptance due to the lack of a physical mechanism that can couple the IMF with the solar interior. However, we can consider that the poloidal field, which stretches from pole to pole through the interior, can pick up *g-modes* through interaction at the base of the convection zone. The field lines can then launch Alfvén

waves towards the solar surface. Even assuming for strong reflection at the level where the plasma beta changes from  $> 1$  to  $< 1$ , we can expect to see the Alfvén waves with *g-mode* frequencies in the coronal field, especially near the poles. Since theoretical amplitudes are not available, one must literally “hunt” for the lowest detectable amplitude of the Alfvén waves at the *g-mode* frequencies. Since the periods of these modes are larger than 30 minutes and lie in the region of hours, we expect to go very faint with large enough integration. We thus need a platform of exceptional stability, and hence need to go to space. Needless to say, detection of solar *g-modes* is a much sought after prize in solar physics and is therefore an ideal goal for cosmic vision.

**Observational requirement:** *Magnetic and velocity oscillations. High sensitivity magnetic and Doppler observation, with a cadence better than the g-mode period. Again, this could be achieved by high sensitivity Stokes spectro-polarimetry in a chosen coronal emission line.*

#### 4. Suitability of Fe XIII (1.0746 $\mu$ m) line for coronal magnetic field measurement

There are number of well known forbidden emission lines originating in the solar corona which could be used for the magnetic field measurements. Examples are green and red lines of Fe X IV (0.530 $\mu$ m) and Fe X (0.637 $\mu$ m) in the visible and Fe X III (1.075 $\mu$ m) line in the infrared. Measurement of full Stokes vector of these lines can give information on the line-of-sight field strength through longitudinal Zeeman effect (Stokes *V*) and the direction of the vector field projected onto the plane-of-the-sky (Stokes *Q*, and *U*) through the resonance scattering induced linear polarization (“strong field” regime of the Hanle effect).

Magnetic sensitivity is an important factor in selecting the coronal line. The Zeeman splitting in a spectral line is proportional to the square of the wavelength ( $\Delta\lambda \propto \lambda^2 B$ ). This gives an advantage of using infrared lines over visible for the weak coronal magnetic field measurements. For example, infrared Fe X III (1.075 $\mu$ m) line is around 4 times more sensitive to magnetic field than the visible Fe X IV (0.530 $\mu$ m) line. More over, contribution from F and K corona, which appear as background intensity, is smaller in infrared. Fe X III at 1.075 $\mu$ m is one of the most suitable and tested (Lin et al.<sup>[6]</sup>) with SOLAR-C telescope line for the coronal magnetic field measurement and is also one of the strongest emission lines identified in the infrared. The important properties of this line are listed in table 1.

**Table 1.** *Important properties of Fe X III coronal emission line*

|                                  |  |
|----------------------------------|--|
| Wavelength                       | 1.0746 $\mu$ m   |
| Landé factor ( <i>g</i> -factor) | 1.5  |
| Transition                       | $3s^2 3p^2 \ ^3P_1 \rightarrow 3s^2 3p^2 \ ^3P_0$                        |
| Line intensity (theoretical)     | $21 \text{ erg cm}^{-1} \text{ s}^{-1} \text{ \AA}^{-1} \text{ sr}^{-1}$ |
| Formation temperature            | $\sim 1.7 \text{ MK}$  |

Figure 4 show the merit of various coronal emission lines according to a study conducted by Judge et al.<sup>[1]</sup> showing as a function wavelength. They concluded that Fe X III (1.075  $\mu\text{m}$ ) is one of the best candidates for the coronal magnetic field measurements.

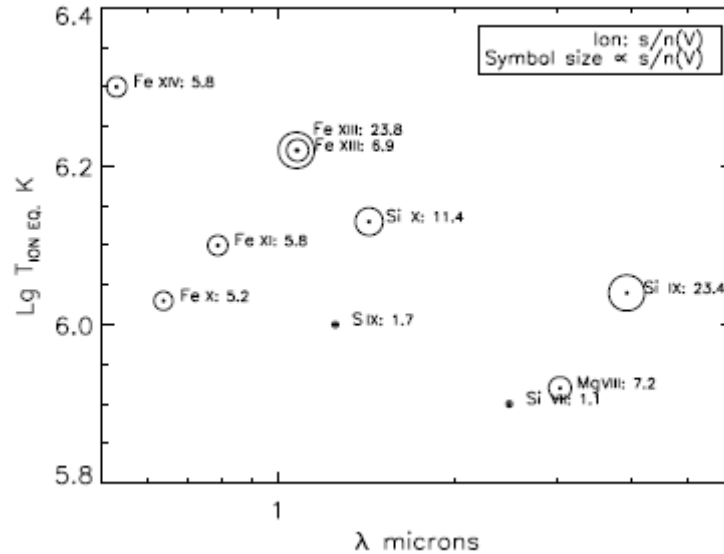


**Fig. 4.** Merit of emission lines as a function of wavelength and formation temperature on the basis of signal to noise ratio of the Stokes V profiles.

**Summary:** The well-tested Fe XIII (1.075 $\mu\text{m}$ ) infrared coronal emission line can be used for coronal magnetic field measurements, taking advantage of its relatively higher Zeeman sensitivity and line strength

## 5. Expected polarization signals from Fe X III coronal line

In corona, the Zeeman splitting is much smaller than the Doppler width of the line profile and the weak field approximation is valid. Thus the observed Stokes V signal (which is proportional to the first derivative of the intensity profile) can be related to the line-of-sight magnetic field strength using the magnetograph formula,

$$V_{\lambda} = 4.67 \times 10^{-13} g B_{LOS} \lambda^2 dI_{\lambda} / d\lambda$$

Where,  $g$  is the Landé factor for the transition,  $B_{LOS}$  (in Gauss) is the line-of-sight magnetic field strength, and  $dI_{\lambda}/d\lambda$  is the slope of the emission line profile at wavelength  $\lambda$  (in  $\text{\AA}$ ). Note that this equation assumes a magnetic fill-factor of 1, i.e. is completely resolved. Figure 5 shows a simple simulation for the expected Stokes V signal in the Fe X III line for magnetic field strengths ranging from 1 – 10 G. Here, a Gaussian profile of FWHM of 30km/s is assumed for the emission line. As it is evident in the figure, 1G field in the corona produces a Stokes V signal of only around  $10^{-4}$  in the Fe X III line.

Achieving this kind of polarization accuracy with very low intensities available in the corona is one of greatest challenges in the coronal magnetic field measurements.

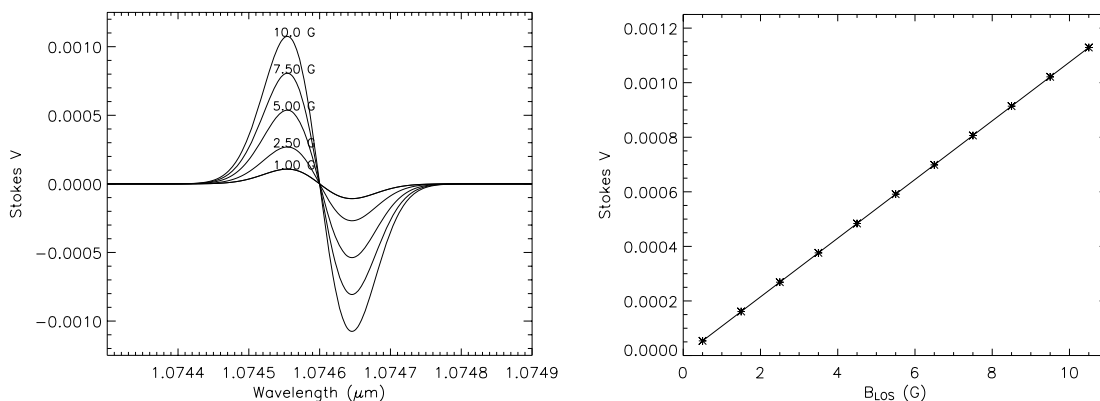


**Fig. 5.** (left) Computed Stokes profiles for various line-of-sight magnetic field strengths, (right) expected maximum Stokes V signal versus magnetic field strength.

The linear polarization signal originating from the resonance scattering, bearing information only on the orientation of the field vector in plane-of-the sky, have much higher amplitudes and is the main contributor for the Stokes  $Q$ ,  $U$  signals. The expected values originating from the resonance scattering polarization process are  $\sim 0.01$  to  $0.1$ , and is much more easier to measure than the Stokes  $V$  signal.

**Summary:** The expected Stokes  $V$  signal, for a fully resolved field line, from Fe XIII ( $1.075\mu\text{m}$ ) infrared coronal emission line vary from  $10^{-4}$  to  $10^{-3}$  for line-of-sight fields of  $1 - 10$  G, respectively. The linear polarization signal is much higher ( $0.1 - 0.01$ ) and carry information only about the POS magnetic field orientation

## 6. Polarization measurement technique

Employing simple but sensitive Stokes polarimetry, it is possible to retrieve the line-of-sight field strength (through Zeeman effect) and the plane-of-the-sky (POS) orientation of the magnetic field (through resonance scattering). In order to obtain the full vector magnetic field, one should measure polarization state of the spectral line, i.e. all Stokes parameters  $I$ ,  $Q$ ,  $U$  and  $V$ . Stokes  $I$  gives the total intensity,  $V$  gives the circular polarization of the line, which is related to the line-of-sight magnetic field, while  $Q$  and  $U$  give the linear polarization which is related POS orientation of the field. In principle, using a combination of two variable retarders and a linear polarizer it should be possible to modulate the incoming polarization such that all the Stokes parameters could be retrieved from the measurements.

Liquid crystal variable retarders (LCVRs) are successfully used for polarization measurements in infrared. This has advantage of no moving parts and can be tuned to different retardance by applying low voltages. Figure 6 shows a configuration of the modulator which uses two LCVRs ( $LC1$  and  $LC2$  with retardance  $\delta 1$  and  $\delta 2$ ,

respectively) with its fast axis aligned at  $0^\circ$  and  $45^\circ$  to the linear polarizer axis ( $LP$ ). In this configuration the detected intensity is a linear combination of the Stokes parameters as given by,

$$I_D = I + C_{\delta_2}Q + S_{\delta_1}S_{\delta_2}U - C_{\delta_1}S_{\delta_2}V$$

$$C_{\delta_1} = \cos(\delta_1), S_{\delta_1} = \sin(\delta_1)$$

$$C_{\delta_2} = \cos(\delta_2), S_{\delta_2} = \sin(\delta_2)$$

For the vector mode, six independent linear combinations can be obtained from which all four Stokes parameters can be retrieved. This could be achieved by setting the retardance of first and second LCVRs as  $\delta I = [0,0,0,0,90,90]$  and  $\delta 2 = [270,90,0,180,90,270]$  for obtaining  $I+V$ ,  $I-V$ ,  $I+Q$ ,  $I-Q$ ,  $I+U$  and  $I-U$ , respectively.

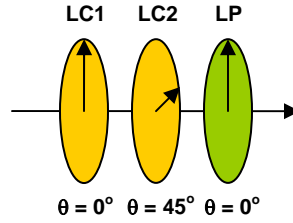


**Fig. 6.** Polarization modulation scheme using two liquid crystal variable retarders, the fast axis of which are oriented at  $0^\circ$  and  $45^\circ$  to the transmission axis of the linear polarizer.

Polarimetric calibration (response) of the instrument is required to convert the measured Stokes parameters into the real Stokes vectors<sup>[21]</sup>. This is very important in the coronal magnetic field measurement due to the stringent polarimetric accuracy (of the order of  $10^{-4}$ ) required in retrieving the magnetic field. The polarimetric response of the instrument can be written as,

$$S_{meas} = RS_{input}$$

Where  $S_{input}$  is the Stokes vector input into the polarimeter,  $S_{meas}$  is the measured Stokes vector,  $R$  is the  $4 \times 4$  element response which relates the two. An ideal polarimeter will have a response matrix which approaches to unity, the off-diagonal elements represent the cross-talk between the Stokes states introduced by the instrument. The response matrix of the modulation package can be determined from the measured Stokes parameters of the exactly known input polarizations, which can be obtained by introducing a combination of linear polarizer and a circular polarizer (quarter wave plate). Taking measurements with out the polarizer and quarter wave plates in the beam, with the polarizer at  $0, 45, 90$  and  $135$  ( $I+Q, I+U, I-Q$  and  $I+Q$ ) degrees and with the quarter wave plate fixed at  $0^\circ$  and the polarizer at  $\pm 45^\circ$  ( $I+V$  and  $I-V$ ), it would be possible to compute the response matrix. Once the response matrix is known from the measured input Stokes parameters, the real Stokes parameters can be obtained as,

$$S_{input} = R^{-1}S_{meas}$$

The requirement of accuracy of the response matrix can be determined from the expected signals from the corona. Given the expected values of the linear polarization of 10% and a magnetic field strength of 10 G, the Stokes vector from the corona can be written as,

$$S_{corona} = \begin{bmatrix} 1 \\ 0.1 \\ 0.1 \\ 10^{-3} \end{bmatrix}$$

The acceptable noise level for the calibrated Stokes vector to observe  $I$ ,  $Q$ , and  $U$  with an accuracy of  $10^{-3}$  and  $V$  to an equivalent precision of 1G corresponding to a signal of  $10^{-4}$ , the Stokes noise vector should be,

$$\sigma_s \leq \begin{bmatrix} 10^{-3} \\ 10^{-3} \\ 10^{-3} \\ 10^{-4} \end{bmatrix}$$

Using  $S_{corona}$  as the input and  $\sigma_s$  for the output we can show that the acceptable errors on the response matrix elements are of the order of,

$$\sigma_s \leq \begin{bmatrix} - & 10^{-2} & 10^{-2} & 10^0 \\ 10^{-3} & 10^{-2} & 10^{-2} & 10^0 \\ 10^{-3} & 10^{-2} & 10^{-2} & 10^0 \\ 10^{-4} & 10^{-3} & 10^{-3} & 10^{-1} \end{bmatrix}$$

Tomczyk et al.<sup>[21]</sup> showed that the above mentioned precision can be achieved using the modulation schemes using LCVRs and linear-polarizer, except in the fourth row of the matrix which gives the cross-talk of Stokes  $I$ ,  $Q$  and  $U$  into  $V$ . In their simulation, for field strength of 1G or less the above cross-talk dominates. This emphasizes the need for accurate polarimetry i.e. the polarization contamination from the telescope and other auxiliary instruments should be less than  $10^{-4}$ .

The first step in the measurement of magnetic field is the selection of the emission line. As we pointed out earlier, Fe X III is one of the best candidates for our purpose. The next step is to obtain all the four Stokes parameters ( $I_\lambda, Q_\lambda, U_\lambda, V_\lambda$ ) for each selected wavelength across the line profile. The cross-talk originating in the modulation process and from the telescope should be corrected before retrieving the magnetic field strength and POS orientation from the Stokes parameters.  $B_{LOS}$ , linear polarization

( $P = \sqrt{Q^2 + U^2}/I$ ) and azimuth ( $\phi = \frac{1}{2} \tan^{-1}(U/Q)$ ) of the magnetic field can be determined by non linear least-squares fit assuming Gaussian profiles for Stokes  $I$ ,  $Q$ , and  $U$  and  $V$  profile given by the first order derivative of a Gaussian<sup>[21]</sup>.

**Summary:** *A modulation scheme using LCVRs and a linear polarizer can be used for the measurement all the Stokes parameters with minimal cross-talk. From the cross-talk corrected Stoke  $I$ ,  $Q$ ,  $U$  and  $V$  profiles, it would be possible to retrieve the line-of-sight field and the POS orientation*

## 7. Wavelength selection: Narrow band tunable birefringent filter

For wavelength selection, a spectrograph or a narrow-band filter could be used. Spectrograph can provide higher wavelength resolution and the full-line profile over the narrow-band filter. But, given the weak field nature of the coronal magnetic field measurements, a coronal magnetograph can constrain the line-of-sight field strength and POS directions with as few as three spectral resolution elements over the line profile. Given the small number of required spectral measurements, a filter based instrument could provide higher through-put (depending upon the pass-band) and thus can considerably reduce the exposure times.

Recently Tomczyk et al.<sup>[21]</sup> showed that a tunable birefringent Lyot filter with a FWHM of  $1.3\text{\AA}$  (with a pass-band displacement of  $\pm 780\text{m\AA}$  to the line wing) can provide enough sensitivity in Stokes  $V$  signal required for the coronal magnetic field measurements. Figure 7 shows the optical components and the transmission profiles of the filter used in their measurements.

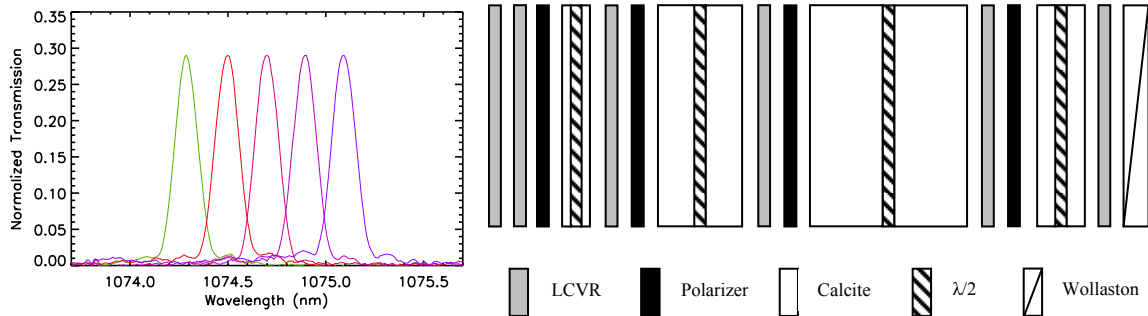


**Fig. 7.** (left) *The transmission profiles of the tunable birefringent filter used by Tomczyk et al.<sup>[21]</sup> for coronal magnetic field measurements, tuned to five different positions in wavelength each shifted by  $2\text{\AA}$*  (right) *The construction details of the filter.*

This filter has wide-field imaging capability which is an advantage for the large field-of-view encountered in the coronal observations. The filter is tunable and the tuning is accomplished by low voltages applied to the LCVRs. The total transmission of the filter is around 30%. Evaluating the characteristics of this filter, we conclude that the birefringent tunable Lyot filter discussed above is an ideal solution for isolating the coronal emission line profile.

**Summary:** *Evaluating the characteristics of the tunable birefringent filter used in coronal magnetic field measurements by Tomczyk et al.<sup>[21]</sup>, we conclude that this is an ideal solution for isolating the emission line profile in filter based magnetograph*

## 8. Photon budget and exposure time estimation

For the estimation of photon flux budget, we use the following parameters which will be realized in our proposed coronagraph;

|   |   |
|---|---|
| Collecting area ( $A$ )                   | : 1963 cm <sup>2</sup> (corresponds to 50cm unobstructed aperture)              |
| Intensity in Fe XIII line ( $I$ )         | : $1.1 \times 10^{12}$ photons/cm <sup>2</sup> /s/sr (at 1.1 R <sub>sun</sub> ) |
| Doppler width of the line ( $\lambda_D$ ) | : 30 km/s   |
| FWHM of the filter ( $\Delta\lambda$ )    | : 1.3 Å   |
| Efficiency of the system ( $\tau$ )       | : 15% (including the detector efficiency)                                       |
| CCD size                                  | : 2048 × 2048 (assuming a Teledyne Hawaii-2RG, IR)                              |
| Plate scale ( $\Delta x$ )                | : 2.8 arc-sec/pix (corresponding to 6R <sub>sun</sub> )                         |
| QE of CCD ( $QE$ )                        | : 65%   |
| Full-well capacity ( $fwc$ )              | : 100 ke <sup>-</sup>   |

For the above parameters of the telescope, the total number of photons collected per second is given by,

$$N_I = I \cdot \Delta x^2 \cdot \Delta \lambda \cdot \tau \cdot A \approx 7.2 \times 10^4 \text{ photons}$$

The above number of photons is applicable to the *Stokes I* measurements. For *Stokes Q*, *U* and *V* parameters, each requires two measurements. For example, in *I+V* measurement since  $|V| \ll |I|$ , we can equate  $N_{I+V} \approx N_I$ , and the photon noise resulting from this measurement to  $\sigma_{I+V} = \sqrt{N_I}$ . The uncertainties in *V* (and also in *Q* and *U*) must be evaluated from error propagation rules, since *V* is computed as  $\frac{1}{2}(I + V) - \frac{1}{2}(I - V)$ . This gives the square of the uncertainty *V* as,

$$\sigma_V^2 = \frac{1}{4}\sigma_{i+v}^2 + \frac{1}{4}\sigma_{i-v}^2 \approx \frac{1}{2}N_I$$

We can express the maximum *V* signal as  $\max(|V|) = \epsilon_v I$ , where  $\epsilon_v$  is the parameter for the expected signal in terms *I*. So the peak signal to noise ratio for *V* can be written as,

$$\frac{V}{\sigma_V} = \frac{\epsilon_v N_I}{\sqrt{N_I/2}} \approx \epsilon_v \sqrt{2N_I}$$

For  $3\sigma$  detection of  $\epsilon_v = 10^{-3}$  ( $B_{LOS} \approx 10G$ ) the number of photons required would be  $4.5 \times 10^6$  counts, which in our case could be achieved with an integration time of 63 seconds

each for  $(I+V)$  and  $(I-V)$  signals. Similarly the integration time for  $3\sigma$  detection of  $\varepsilon_v = 10^{-4}$  ( $B_{LOS} \approx 1G$ ) would be around 105 min.

**Summary:** *With a 50 cm telescope and 63 seconds of integration time, a  $3\sigma$  detection of 10 G field with a spatial resolution of 2.8 arc-sec/pixel is possible. For 1G field the integration time would be around 105 minutes*

## 9. Preliminary optical design of the coronagraph

In this section we present a preliminary design of a spaced based coronagraph and the magnetograph. We also provide an approximate estimate of the weight for the entire system. Please note that, this is a preliminary concept and could be greatly improved by optimizing the optical design.

### 9.1. Telescope (Coronagraph)

Figure 8 shows the conceptual design (using Zemax optical software) of the proposed coronagraph. The entrance aperture of 500mm allows the full sun and the corona to fall on the off-axis parabolic mirror (M1) of 550mm clear aperture with an off-axis distance of 438mm. The 1250mm focal length mirror provides a primary beam with an f-number of 2.5. The image quality and size at the primary image plane suffer from the aberrations introduced by the mirror M1; coma being the dominant error. Image size of the full solar disk and the corona at the primary focal plane are 12.8mm and 38.3mm, respectively (corresponding to a total field-of-view of  $6R_{sun}$ ). Zerodur material is used for the primary mirror due to its small thermal expansion coefficient.

Using a tilted mirror M2 with a central hole, the coronal light is reflected to an appropriate direction for collimation and imaging. Since the mirror M2 is tilted ( $\approx 19.8^\circ$ ) with respect to the primary image plane, the (projected) image sizes of the corona and solar disk are slightly different. The diameter of the hole required in the secondary mirror M2 to remove the solar disk light is around 15.3mm, with an overall size of 43.8mm for M2 to reflect  $6R_{sun}$  coronal field-of-view. The rejected solar disk light can be taken out of the telescope using a third mirror M3. The introduction of the tilted mirror at the primary image plane causes vignetting and degrades the image quality. The reflected light from M2 corresponds to a coronal field-of-view of 1.05 to 3 solar radii.

To compensate the error induced by the primary mirror M1, an off-axis parabolic mirror (M4) of diameter 200mm with an off-axis distance of 131mm is used, which also acts like a collimator. Focal length of this mirror is 375mm. This mirror forms an image of the entrance pupil at a distance of 411mm. To remove the diffraction effects introduced by the edges of the entrance aperture, a Lyot stop is placed at this location.

Off-axis-parabolic mirror M5 (off-axis distance of 175mm and diameter 225mm) together with lens L1 forms an image of coronal field-of-view at F2. The polarimeter and the narrow band filter is placed in this telecentric beam. The combination of lenses L2

and L3 forms a coronal image of an appropriate size at F3 where the CCD is placed. The final image size is 37mm for  $6R_{\text{sun}}$  field-of-view which exactly fits into a CCD of  $2048 \times 2048$  pixels with  $18\mu\text{m}$  pixel size (fill factor of 98% is assumed). At the image plane a 2.84arc-sec/pixel resolution is achieved with this configuration. The salient features of the telescope are given in Table 2.

**Table 2.** *Salient features of the coronagraph*

|                    |   |
|--------------------|---|
| Entrance aperture  | 500 mm  |
| Field-of-view      | 1.05 to 3.0 solar radii   |
| Primary mirror     | Off-axis parabolic, $\Phi = 550\text{mm}$ , $f = 1250\text{mm}$ , off-axis distance = 437.5 mm          |
| Occluder           | Internal, secondary mirror with a hole, $\Phi = 15.3$ mm  |
| Collimating mirror | $\Phi = 200\text{mm}$ , $f = 375\text{mm}$ , OAP, off-axis distance = 131.25 mm                         |
| Lyot-stop          | Inner diameter = 165 mm, $\Phi = 200\text{mm}$  |
| Folding mirror     | $\Phi = 230\text{mm}$ , $f = 750$ mm, OAP, off-axis distance = 175                                      |
| Lens L1            | $\Phi = 110\text{mm}$ , Material : SF57   |
| Imaging lenses     | L2, $\Phi = 110\text{mm}$ , Material : SF57<br>L3, assumed as thin lenses<br>L4, assumed as thin lenses |
| CCD                | $2048 \times 2048$ , pixel size = 18 micron. Fill factor = 98%  |
| Resolution         | 2.84 arc-sec/pixel  |

## 9.2. Back end instrument (Coronal vector magnetograph)

The back end instrument consists of the following components,

- i) Calibration optics
- ii) Polarimeter
- iii) Narrow band filter
- iv) IR detector

### 9.2.1. Calibration optics

An insertable diffuser in the pupil plane near the Lyot stop will be used for intensity calibrations. Diffusers are available with wide scatter angle (such as Light shaping diffuser from Physical Optics Corporation with  $40^\circ$  FWHM) which produces uniform intensity for our field-of-view. The diffuser will be used a) for obtaining the flat field image which removes the pixel-to-pixel detector sensitivity variations, b) normalization of the Lyot filter transmission at different wavelength positions, and c) normalization of the observed intensity to solar disk units.

Polarimeter calibration unit consists of an insertable precise linear polarizer on a rotating stage and an insertable true zero-order quarter wave plate. This mechanism will be used for determining the response function of the polarimeter by taking the calibration images (for the linear polarization) through the polarizer at 0, 45, 90 and 135 degrees

orientations. The circular polarization calibration images will be obtained by fixing the fast axis of the quarter wave plate at 0 degrees and the linear polarizer  $\pm 45$  degrees. The above set of measurement will provide the response matrix for the polarimeter unit.

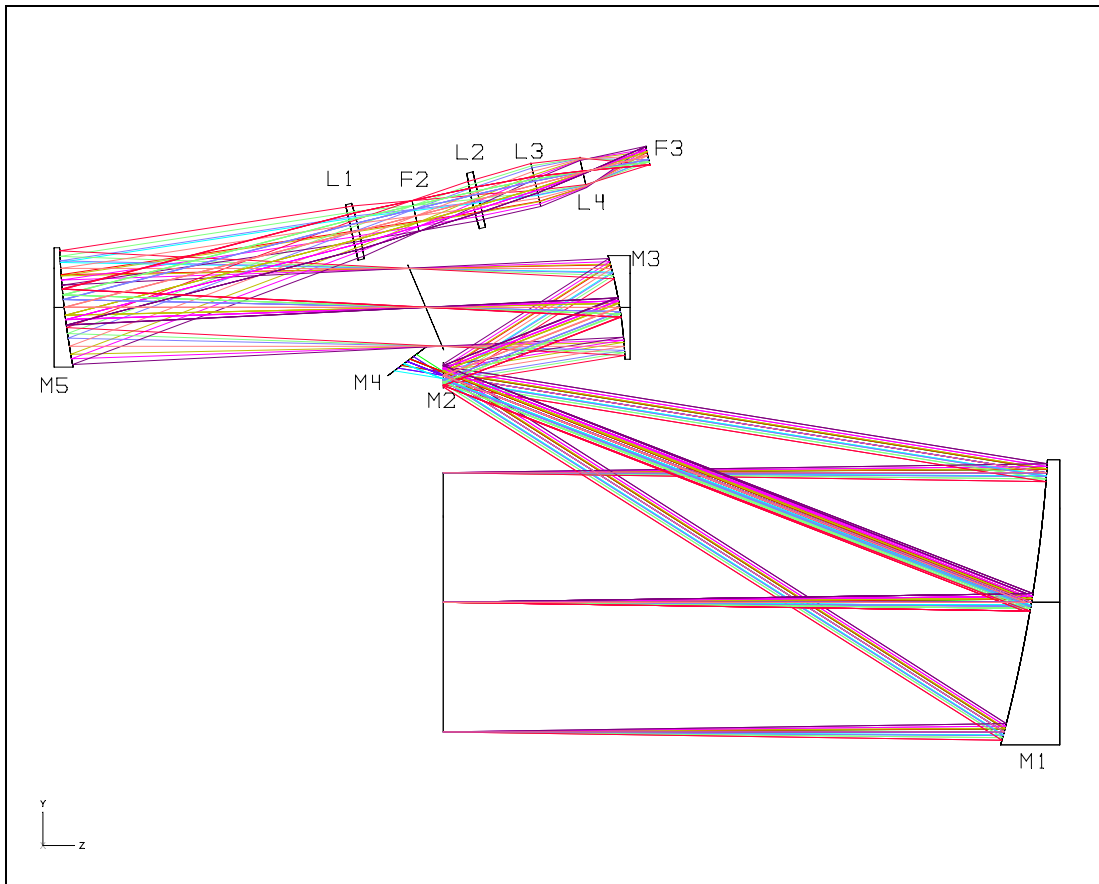


**Fig. 8.** *The preliminary optical design of the coronagraph telescope. The calibration unit, polarimeter, and the narrow band filter will be placed between lenses L1 and L2*

### 9.2.2. Polarimeter

The polarimeter consist of two liquid crystal variable retarders (LCVRs) and a linear polarizer placed with its fast and transmission axes aligned as shown in figure 6. In LCVRs the retardance can be varied by applying low voltages (in the range 0 to 20 Volts), and thus can be tuned to provide to provide  $\pm\lambda/4$  or  $\lambda/2$  retardance. The sequence of retardance for obtaining all the Stokes parameters is discussed in the earlier section.

### 9.2.3. Narrow band filter

A Lyot birefringent filter with a passband of  $1.3\text{\AA}$  will be used for selecting the emission line. The construction details of the above filter are shown in figure 7. This is a four stage birefringent filter, with wide-field capability. LCVRs placed in between the calcite

crystals are used for tuning the filter to different wavelength positions. The use of LCVRs makes the filter electrically tunable.

#### **9.2.4. IR detector**

A  $2048 \times 2048$  infrared CCD camera (similar to the Teledyne HAWAII – 2RG) will be used for the coronal imaging. The camera is available with  $18 \mu\text{m}$  pixels and 65% quantum efficiency. The camera needs liquid nitrogen cooling below 30K and has a full well capacity of  $100 \text{ ke}^-$ . The plate scale at the camera plane is around 2.8 arc-sec/pixel, which is sufficient for our observations.

#### **9.2.5. Instrument control and data acquisition system**

The instrument control unit can be an onboard computer which supervises various instrument controllers based upon the commands received from ground or in autonomous mode. The instrument controllers will be dedicated to specific systems such as polarimeter control, filter tuning electronics, thermal control etc. The data acquisition system will be integrated with the IR detector and the instrument control and a data storage unit.

**Summary:** *A 50cm off-axis coronagraph telescope is proposed for the space based coronal magnetic field measurements. A filter based polarimeter and IR detector is used for this purpose*

## **12. Satellite requirements**

A satellite in the circular polar Sun-synchronous orbit (around 600km, similar to *Solar – B* orbit) will be ideal for our observations. This orbit has advantage of continuous solar viewing for approximately eight months, followed by four months with short eclipse periods (upto 20min). From the preliminary optical design of the telescope we obtain a size of  $2\text{m} \times 1.5\text{m} \times 0.65\text{m}$  for the payload (the major unknown being the dimensions of the IR camera system, which needs to be cooled to liquid nitrogen temperatures). The total mass of the optical components including the primary mirror (assuming Zerodur material) will be around 50Kg and we presume a mass of 300Kg for the support structure and the cooling system for the camera (e.g. nitrogen ice dewar, in the case of Hubble Space Telescope NICMOS IR camera the weight of the nitrogen ice was around 104Kg). So, the approximate total weight would be in the range of 350Kg. The main power consumption will be by the CCD camera, data acquisition and instrument control units. 100 – 150 watts power will be sufficient for this purpose. We envisage a pointing accuracy of better than 1 arc-sec for the satellite.

**Summary:** *A satellite in polar Sun-synchronous orbit with a payload capability of 350Kg is envisaged for this project*

### 13. Time schedule

The project will be carried out in three phases. In the first phase (2008 – 2009) the exact instrument specifications will be worked out for the science goals detailed in Section 2. For example, a thorough comparison of a spectrograph and filter based system for the coronal magnetic field measurement will be carried out and the selection of the instrument will be done accordingly. The study will be carried out on the basis of observational data, that will be made available using recently installed coronal magnetographs – namely SOLAR-C/OFIS<sup>[6]</sup> and CoMP<sup>[21]</sup>. These two magnetographs measure the coronal magnetic field using spectrograph and filter based techniques. This study will be complemented by evaluating the theoretical performance of the above two systems in precise coronal magnetic field measurements.

In second phase (2009 – 2012), optical design of the telescope and the magnetograph will be finalized. Procuring of the components and also, the prototype (flight model) instrument will be realized during this phase. In the third phase the (2012 – 2015) the payload will be developed, tested and calibrated and will be ready for flight by 2016.

**Summary:** *The project will be carried out in three phases, (2008 – 2009) definition of exact instrument specification, (2009 – 2012) optical design, procuring of components and prototype development, (2012 – 2015) payload development, (2016) completed payload*

#### References:

- [1] *Coronal magnetometry: A feasibility study*, P. G. Judge, R. Casini, S. Tomczyk, D. P. Edwards, E. Francis, 2001, NCAR Technical note, **NCAR/TN-466+STR**
- [2] *Solar coronal magnetic field mapper*, S. K. Solanki, N. –E. Raouafi, A. Gandorfer, U. Schuhle, and A. Lagg, 2006, **ESA SP-617**
- [3] *Ph. D Thesis*, J. W. Harvey, 1969, University of Boulder
- [4] *Infrared coronal magnetic field measurements*, J. R. Khun, 1995, in J. R. Khun and M. J. Penn (Eds.), *IR Tools for Solar Astrophysics: What is next?*, World Scientific, Singapore, 89
- [5] *A new precise measurement of the coronal magnetic field strength*, H. Lin, M. J. Penn, and S. Tomczyk, 2000, *ApJ*, **541**, L83
- [6] *Coronal magnetic field measurements*, H. Lin, J. R. Khun, and R. Coulter, 2004, *ApJ*, **613**, L177
- [7] *Spectral lines for polarization measurements of the coronal magnetic field. I. Theoretical intensities*, P. G. Judge, 1998, *ApJ*, **500**, 1009
- [8] *Spectral lines for polarization measurements of the coronal magnetic field. II. Consistent treatment of the Stokes vector for magnetic dipole transitions*, R. Casini, and P. G. Judge, 1999, *ApJ*, **522**, 524
- [9] *Spectral lines for polarization measurements of the coronal magnetic field. III. Atomic data for Si IX*, T. Barge, P. G. Judge, P. Jonsson, and D. P. Edwards, 2000, *ApJ*, **540**, 1114

- [10] *Spectral lines for polarization measurements of the coronal magnetic field. IV. Stokes signals in current carrying fields*, P. G. Judge, B. C. Low, and R. Casini, 2006, **651**, 1229
- [11] *Coronal Mass Ejection: Initiation, magnetic helicity and flux ropes. I. Boundary motion driven evolution*, T. Amari, J. F. Luciani, J. J. Aly, Z. Mikic, and J. Linker, 2003, ApJ, **585**, 1073
- [12] *The hydromagnetic nature of solar coronal mass ejections*, M. Zhang, and B. C. Low, 2005, Annu. Rev. Astron. Astrophys., **43**, 103
- [13] *Magnetic causes of solar coronal mass ejections: Dominance of the free magnetic energy over the magnetic twist alone*, D. A. Falconer, R. L. Moore, and G. A. Gary, 2006, ApJ, **644**, 1258
- [14] *Sigmoidal morphology and eruptive solar activity*, R. C. Canfield, H. S. Hudson, and D. E. McKenzie, 1999, GeoRL, **26**, 627
- [15] *Physics of the solar corona*, M. Aschwanden, 2006, Springer-Praxis Publishing
- [16] *Magnetic neutral sheets in evolving fields. I - General theory. II - Formation of the solar corona*, E. N. Parker, 1983, ApJ, **264**, 642
- [17] *On heating the Sun's corona by magnetic explosions: Feasibility in active regions and prospects for quiet regions and coronal holes*, R. L. Moore, D. A. Falconer, J. G. Porter and S. T. Suess, 1999, ApJ, **526**, 505
- [18] *An assessment of magnetic conditions for strong coronal heating in solar active regions by comparing observed loops with computed potential field lines*, D. A. Falconer, G. A. Gary, R. L. Moore, and J. G. Porter, 2000, ApJ, **528**, 1004
- [19] *On cross-spectrum capabilities for detecting stellar oscillation modes*, T. Appourchaux, J. Leibacher, P. Boumier, 2007, A&A, **463**, 1211
- [20] *Power spectral density of electron flux from Ulysses, 1999-2001*, D. J. Thomson, C. G. MacLennan, L. J. Lanzerotti, 2003, ESA **SP-517**, 401
- [21] *An instrument to measure coronal emission line polarization*, S. Tomczyk, G. L. Card, T. Darnell, D. F. Elmore et al., HAO (the exact details not available)